Growing Pollen Tubes Possess a Constitutive Alkaline Band in the Clear Zone and a Growth-dependent Acidic Tip

J.A. Feijó,*‡ J. Sainhas,‡ G.R. Hackett,§ J.G. Kunkel,§ and P.K. Hepler§

*Department Biologia Vegetal, Faculdade de Ciências, Universidade de Lisboa, P-1749-016 Lisboa, Portugal; ‡Gulbenkian Institute of Science, P-2780-156 Oeiras, Portugal; and §Biology Department and Plant Biology Graduate Program, Morrill Science Center, University of Massachusetts, Amherst, Massachusetts 01003

Abstract. Using both the proton selective vibrating electrode to probe the extracellular currents and ratiometric wide-field fluorescence microscopy with the indicator 2′,7′-bis-(2-carboxyethyl)-5-(and-6)-carboxyfluorescein (BCECF)-dextran to image the intracellular pH, we have examined the distribution and activity of protons (H^+) associated with pollen tube growth. The intracellular images reveal that lily pollen tubes possess a constitutive alkaline band at the base of the clear zone and an acidic domain at the extreme apex. The extracellular observations, in close agreement, show a proton influx at the extreme apex of the pollen tube and an efflux in the region that corresponds to the position of the alkaline band. The ability to detect the intracellular pH gradient is strongly dependent on the concentration of exogenous buffers in the cytoplasm. Thus, even the indicator dye, if introduced at levels estimated to be of 1.0 μM or greater, will dissipate the gradient, possibly through shuttle buffering. The apical acidic domain correlates closely with the process of growth, and thus may play a direct role, possibly in facilitating vesicle movement and exocytosis. The alkaline band correlates with the position of the reverse fountain streaming at the base of the clear zone, and may participate in the regulation of actin filament formation through the modulation of pH-sensitive actin binding proteins. These studies not only demonstrate that proton gradients exist, but that they may be intimately associated with polarized pollen tube growth.

Key words: pollen tube growth • pH • proton flux • ratiometric ion imaging • vibrating probe

Despite considerable effort to measure and image cytosolic pH (pH_c),[1] a generalized understanding of the status and role of protons in cellular physiology remains elusive. Yet pH_c plays a central role in the regulation of a number of cellular processes including modulation of enzyme activity (Guern et al., 1991), state of phosphorylation (Blowers and Trewavas, 1989), structure and activity of the cytoskeleton (Yonezawa et al., 1985; Suprenant, 1991; Andersland and Parthasarathy, 1993; Edmonds et al., 1995), endocytosis and exocytosis (Cosson et al., 1989; Gluck et al., 1982), and protein synthesis and cell division (Dube et al., 1991; Grandin et al., 1991). The importance of these processes allows the prediction that protons might be one of the most basic and effective common denominators to convey spatial and temporal information inside a living cell, and leads to the notion that modulation of pH_c acts as a bona fide second messenger (Felle, 1989). However, this concept still lacks the foundation to be widely accepted.

Recognizing that localized movement and accumulation of ions correlates with the establishment and magnitude of polarity, especially in tip-growing plant cells, we have focused on the elongating pollen tube as a model system to explore the distribution of protons. Most attention thus far has been directed towards calcium ions (Ca^{2+}), which are observed in the form of a "tip-focused" gradient at the extreme apex of the growing pollen tube (Miller et al., 1992; Pierson et al., 1994). Evidence for the intracellular gradient comes directly from the use of intracellular indicators, e.g., fluorescent dyes (Obermeyer and Weisenseel, 1991; Rathore et al., 1991; Miller et al., 1992; Malhó et al., 1994, 1995; Pierson et al., 1994, 1996) and the photoprotein aequorin (Messerli and Robinson, 1997), and indirectly from the use of the ion-selective vibrating electrode, which re-

Address correspondence to P.K. Hepler, Biology Department and Plant Biology Graduate Program, Morrill Science Center, University of Massachusetts, Amherst, MA 01003. Tel.: (413) 545-2083. Fax: (413) 545-3243. E-mail: jose.feijo@fc.ul.pt or hepler@bio.umass.edu

1. *Abbreviations used in this paper:* ADF, actin-depolymerizing factor; BCECF, 2′,7′-bis-(2-carboxyethyl)-5-(and-6)-carboxyfluorescein; CCD, charge-coupled device; pH_c, cytosolic pH.

veals a flux of Ca^{2+} from the extracellular medium that is inwardly directed specifically at the apex of the pollen tube (Kühtreiber and Jaffe, 1990; Pierson et al., 1994, 1996; Feijó et al., 1994b, 1995).

Although the importance of Ca^{2+} cannot be disputed, it nevertheless seems plausible that other ions, notably protons (H^+), might also be involved, either directly or in concert with Ca^{2+}, as it has been proposed for other polarized growing systems (Felle, 1988a,b). Protons do not possess such low diffusion constants as calcium, however, they do have migration rates that are in the range that allows the theoretical prediction of localized gradients and hot spots, which could act as spatial markers or structural organizers. Moreover, in the pollen system, the H^+-ATPase, as in other plant cells, is the primary electrogenic pump responsible for generating proton gradients that are used by the cell for a myriad of energy requiring processes (Sze, 1985; Al-Awqati, 1986; Briskin and Hanson, 1992). Based on studies with the vibrating electrode and with immuno- and cytochemical probes, the evidence indicates that H^+-ATPases (or their activity) are intrinsically polarized; they are richly expressed in the plasma membrane of the pollen grain, but, with the possible exception of the tip domain, only weakly, if at all, over the pollen tube itself (Weisenseel and Jaffe, 1976; Feijó et al., 1992, 1994a, 1995; Obermeyer et al., 1992).

Less clear is the relationship between H^+ and the process of cell elongation, which is restricted to the extreme apex of the pollen tube. In other tip-growing cells, notably the rhizoid initial of *Pelvetia* (Gibbon and Kropf, 1991, 1994), both H^+-specific microelectrodes and fluorescent indicator dyes indicate that the apex is acidic relative to the bulk cytoplasm with a gradient of 0.3–0.5 U of pH_c. Further studies showed that the acidic tip is necessary for growth, and that axis development starts from small variations in pH_c (Kropf et al., 1995). The evidence from other systems, however, is not as compelling. Negative evidence for an intracellular pH_c gradient has been reported for root hairs (Hermann and Felle, 1995). Fungi, on the other hand, have been the subject of contradictory reports: an alkaline gradient up to 1.4 U has been reported in the growing hyphae of *Neurospora crassa* (Robson et al., 1996), whereas a gradient extending from pH 6.7 in the tip, to above 7.0 and then declining to a basal 6.7 over the first 300 μm has been observed in *Gigaspora margarita* (Jolicoeur et al., 1998). On the other hand Bachewich and Heath (1997) and Parton et al. (1997), using the dye SNARF-1 and confocal microscopy, failed to detect any gradient. However, both groups provided evidence for a role of pH_c in the regulation of hyphal growth.

The evidence is also mixed for studies on pollen tubes themselves. Early work by Turian (1981), using absorbance indicator dyes, reported that the pollen tube apex is acidic. More recently Feijó et al. (1995) provide preliminary evidence showing that some *Agapanthus* pollen tubes have gradients up to 1 pH_c U but, curiously, other pollen tubes do not exhibit any gradient at all, and yet continue to grow. The question has come to an even sharper focus recently with the publication of three studies (Parton et al., 1997; Fricker et al., 1997; Messerli and Robinson, 1998) reporting that in growing pollen tubes pH gradients are not required or associated with tip growth.

Before these recent studies of Parton et al. (1997), Fricker et al. (1997), and Messerli and Robinson (1998) had appeared we too had been working on the question of pH_c gradients associated with pollen tube growth in lily. Using both a proton selective vibrating electrode to probe the extracellular fluxes and ratiometric widefield fluorescence microscopy with the indicator 2′,7′-bis-(2-carboxyethyl)-5-(and-6)-carboxyfluorescein (BCECF)-dextran, to quantitatively image pH_c, we provide evidence that gradients exist. In brief, we show that lily pollen tubes possess a constitutive alkaline band at the base of the clear zone and an acidic domain at the extreme apex. The latter is correlated closely with growth whereas the former, possibly with cytoskeletal dynamics and the presence of membrane H^+-ATPases. These intracellular observations moreover fit closely with the pattern of extracellular currents, showing an H^+ influx at the extreme apex, with efflux at the base of the clear zone, forming a closed loop of proton movement in the tube tip. We conclude, therefore, that proton gradients exist and that they may be associated with polarized pollen tube growth.

Materials and Methods

Pollen Culture

Fresh and liquid nitrogen-stored pollen grains of *Lilium longiflorum* (cv. Ace) were sown in germination medium optimized for the measurement of extracellular proton fluxes with the H^+-selective vibrating probe. More than 10 different media allowed satisfactory results, but all data shown were obtained with medium no. 4, which contained 1.0 mM KCl, 0.05 mM $CaCl_2$, 1.6 mM H_3BO_3, 0.05 mM 2-(*N*-morpholino) ethanesulfonic acid (MES) buffer, and 5% sucrose. All reagents were analytical grade and solutions were made in ultrapure water. Besides providing optimized conditions for the use of the vibrating probe, this medium allowed better growth rates than that previously used for ratiometric studies (Miller et al., 1992; Pierson et al., 1994, 1996). For microinjection, once-germinated pollen tubes were fixed to a coverslip forming the bottom of a microscope slide chamber with a thin layer of medium supplemented with 1.2% low gelling temperature agarose (type VII; Sigma). When the agarose had gelled, the chamber was filled with medium. Measurements were made on tubes 700–2,500 μm in length, with growth rates ranging from 12 to 25 μm/min, and tube diameters ranging from 12 to 18 μm.

Ratiometric pH_c Imaging

Pollen tubes were pressure-injected with BCECF-dextran (10 kD; D-1878; Molecular Probes) diluted to concentrations from 10.0 to 0.5 mg/ml in ultrapure water. Images were captured on a charge-coupled device (CCD) camera (type CH250 camera head, AT 200 camera controller and Thomson TH-7883 CCD chip; Photometrics) attached to a Nikon Diaphot 300 inverted microscope, and using a Nikon 40× 1.3 NA oil immersion objective lens, which has high transmittance. The pollen tubes were illuminated with 450 (pH independent) and 490 nm (pH dependent) light from a mercury arc lamp, which is regulated by a purpose-built power supply. Emitted light was collected at 520 nm. Ratio images were calculated from background-subtracted images of the pH-dependent and -independent wavelengths (490:450 nm), and a threshold applied, such that areas containing little or no dye (low pixel intensity at 450 nm) were set to black. Although the image acquisition software (PMIS; Photometrics) was optimized to collect image pairs at 3–4-s intervals, we were forced, because of low dye concentrations and associated problems of photobleaching, to operate in the range of 15–25-s intervals between successive images. Ratio image and area average calculations were also carried out using PMIS and Comos (v. 6.0; Bio-Rad Microscience). pH was calculated in various parts of the tube by taking an average of a 12 × 12 pixel (~5 μm^2) area.

Both in situ and in vitro calibrations were performed. The in vitro calibration was made with a pseudo-cytosol medium modified from Dixon et al. (1989) containing 100 mM KCl, 30 mM NaCl, 500 mM mannitol, 40% sucrose, 25 mM MES, and 25 mM Hepes, adjusted to pH 6.0, 7.0, and 8.0.

The addition of sucrose allowed for better simulation of the internal viscosity of cells (Poenie, 1990). In situ calibrations were made using a modified protocol from Dixon et al. (1989), Bright et al. (1989), and Kasner and Ganz (1992). Dixon et al. (1989) used a combination of nigericin and elevated extracellular potassium, a protocol that was not entirely successful when used on *Pelvetia* (Kropf et al., 1995). However, when nigericin was combined with valinomycin, as reported by Kasner and Ganz (1992), it was possible to effectively clamp the pH. The final medium was similar to that used for in vitro calibration with 2 μM valinomycin and 5 μM nigericin, and lacking sucrose. In all conditions, deviation between in vitro and in vivo calibration showed less than 0.1 pH U difference at the high pH range (7.5–8.0) and even smaller amounts for the rest of the pH range. For this reason, unless otherwise specified, most of the calibrations shown were obtained by the in vitro method.

Estimation of the final intracellular dye concentration involved the quantification of pixel intensity on the independent channel, which was assumed to be an indirect measure of the dye concentration. A linear transect on the midplane, i.e., diameter, along the tube was pixel averaged. Then preparations with the same thickness between slide and coverslip as the tube previously measured were examined with calibrated solutions of known diluted concentrations (e.g., using regular 22-mm coverslips at a volume of 8 μl will create a thickness of 16.5 μm). These were area averaged after excitation under the exact same conditions as the original image to be calibrated. Under these conditions it was shown that: (a) below 30-μm thickness the relation between the thickness and the emitted fluorescence at 450 nm was linear; (b) with a fixed thickness of 20 μm the relation between the dye concentration and the emitted fluorescence was linear; and (c) there was a general agreement between the in vitro and the in situ calibrations (in the worst scenario a shift of 0.1 pH U occurred on the low edge, close to pH 8.0). This method was thus judged to deliver good estimates of the intracellular concentration of the dye and, indirectly, the dilution associated with the process of microinjection.

Pollen Tube Growth and Intracellular pH Manipulation

The inhibition of pollen tube growth and its subsequent recovery was induced in BCECF-dextran loaded cells by a brief exposure to germination medium with 20% sucrose, followed by a return to normal medium. This procedure allowed us to follow the intracellular pH changes, if any, related to growth.

The effect of buffer on pH_c was monitored by injecting a solution of 5 mM of Hepes, pH 7.0, into tubes previously loaded with BCECF-dextran. Care was taken to select tubes that had already exhibited normal growth rates and cytological appearance.

Extracellular Flux Measurements

An ion-selective vibrating electrode (Kühtreiber and Jaffe, 1990; Kochian et al., 1992) was used to measure extracellular proton fluxes in pollen tubes. Electrodes were pulled from 1.5-mm glass capillaries (TW150-4; World Precision Instruments) with a Sutter Flaming Brown (model P-97; Sutter Instrument) electrode puller. These were made hydrophobic by baking at 250°C for at least 2 h followed by exposure to dimethyl-dichlorosilane (D-3879; Sigma) vapor at 250°C for 10 min and further baking for at least 1 h. The electrodes were back-filled with 40 mM KH_2PO_4 and 15 mM NaCl, pH 7.0, to a length of 10 mm from the tip, and then with a 10–15-μm column of pH selective liquid proton exchange cocktail (Hydrogen Ionophore I-cocktail B, no. 95293; Fluka), which was drawn into the tip of the electrode by application of suction to the basal end of the pipette. A Ag/AgCl wire electrode holder (World Precision Instruments) inserted in the back of the electrode established electrical contact with the bathing solution. The ground electrode was a Ag/AgCl half-cell (World Precision Instruments) connected to the solution by a 0.5% agarose bridge containing 3 M KCl. Signals were measured by a purpose built electrometer (Applicable Electronics). Electrode vibration and positioning were achieved with a three-dimensional (3-D) positioner. Data acquisition, preliminary processing, and control of the stepper motor-driven 3-D positioner were done with the program 3DVIS (adapted by J.G. Kunkel from v. 6 of the program DVIS described by Smith et al. [1994]).

The self-referencing vibrating probe oscillates at 0.5–1.0 Hz with an excursion of 10 μm, completing a whole cycle in 1–2 s. At each position the probe records 10 time bins of data. The first three bin averages at each position are discarded allowing the probe to settle after its move, and the remaining seven are averaged. This settled average is then subtracted from each of the bins of data acquired at the next position of the probe; this subtraction represents the self-referencing feature of the probe (each position is referenced to the settled average of the last position). A rolling average of 14 bins (seven at each oscillation extreme) is recorded and timed at the end of its bin. Thus, the maximum offset in time is 1 s. The rolling average includes the self-referenced bin averages from the current bin plus the 13 preceding bins. Strictly speaking, each rolling average is statistically dependent on the last 13 and the next 13 rolling averages to be calculated by virtue of sharing bin averages in their calculation (Holdaway-Clarke et al., 1997).

Proton fluxes at the surface of a pollen tube were measured by vibrating the electrode tip as close as possible to the perpendicular (90°) of the tube surface without touching the tube. The extreme measuring point was positioned to be within 1–3 μm of the tube surface where fluxes are assumed to be uniform (e.g., Smith et al., 1994) by moving the probe by the smallest steps possible (<0.5 μm). Background references were taken at more than 500 μm from any pollen grain or tube and the value subtracted from the surface measurements. The entire setup was built around a Zeiss IM35 inverted microscope, with video camera attached, and connected to a video recorder. Cells selected for measurement were 800–2,500 μm in length, and were growing parallel to the base of the chamber. The growth of the tube was recorded on videotape.

Tube Growth Rate Measurements

The growth rate of pollen tubes was measured from videotape. Frames were captured from video VHS tape at 2–4-s intervals, and the position of the tip as well as the time was recorded for each frame. The rate, calculated from two adjacent frames, was assigned to a time at the midpoint between them. Growth data were aligned with proton flux using a video data inserter that was time-synchronized with the computer clock. Time values were taken directly from the video frames and ASCII files produced by the 3DVIS software.

Results

Proton Extracellular Fluxes Are Organized in Spatially Localized Loops

To characterize proton dynamics and pH regulation in growing pollen tubes, we first examined the extracellular currents using the proton selective vibrating probe. Various reasons underlie this choice; it is a totally noninvasive technique, easy to apply to growing pollen tubes and, with the available pH sensors, has an excellent signal to noise ratio (Kochian et al., 1992). Furthermore, it has already been used to examine proton fluxes around early germinating pollen grains and short tubes (Feijó et al., 1994b). The recent discovery of periodic growth rate oscillation in pollen tubes longer than 700 μm (Pierson et al., 1996) made it pertinent to examine closely their extracellular proton fluxes.

Germinating pollen grains and short tubes (<300 μm) were shown to follow much the same pattern described for total electric currents, i.e., the grain is the only source and the tube is the sink (Feijó et al., 1994b). This pattern was confirmed in the present study. However, tubes were followed to longer lengths, revealing a new, emerging pattern that is depicted in Fig. 1. From 600–800 μm on, we detected a new membrane domain, roughly corresponding to the clear zone, that effluxes. These fluxes, which in some instances attained values (per area unit) similar to those detected in the grain, seemed to be stable, or at least did not exhibit distinct temporal changes. It follows that at this length two closed loops of proton circulation emerged, one around the grain, and another around the growing tip. The bulk of the flux source and sink range to ~150–200 μm in both cases. Although the absolute values of the flux showed some variability from cell to cell, this pattern was

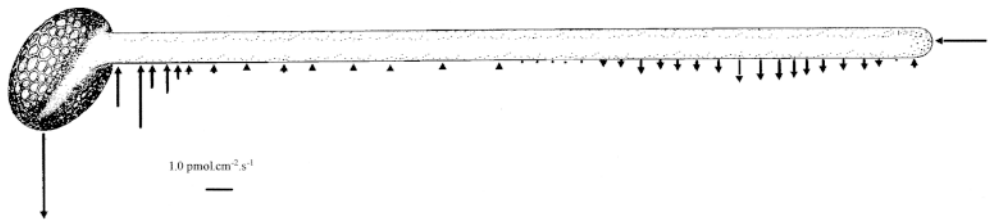

Figure 1. Representative profile of the proton fluxes along a growing pollen tube (~800-μm long) at pH 6.1. The pollen grain membrane always drives significant effluxes of protons, presumably by the activity of proton translocating ATPases located at the pollen grain membrane (see Discussion). Immediately after the pore, pollen tubes show a strong influx domain of protons in the proximal 150–200 μm. This influx decreases along the tube and eventually reverses, becoming a clear efflux of protons in the region of the clear zone. Another reversal of the current direction is observed in the apical dome, characterized by a strong point influx at the very tip, with chaotic small amplitude oscillations for short tubes, or sustained large amplitude oscillations for longer tubes. The clear zone domain of proton efflux is usually not discernible in small tubes (<500 μm), and becomes increasingly well defined from the size of the one depicted. As tubes continue to elongate this pattern evolves subsequently to a banding alternation of small efflux and influx domains over distances of ~300–400 μm. However the grain + proximal tube and the clear zone + tip-closed loops of proton circulation remain as shown in this figure. Although these patterns have been confirmed in a significant number of tubes ($n = 13$) the absolute values shown vary considerably with the bath pH and tube length. Bar, 1.0 pmol/cm^2/s; pollen grain and tube not drawn exactly to scale; grain is ~120 × 80 μm and tube is ~18 μm in diameter.

stable, being confirmed in a significant number of growing tubes ($n = 13$). Between the two loops there was another membrane domain where only very small fluxes were observed. Some of these fluxes revealed significant deviations from the background noise but they cannot be compared in magnitude with the signals detected around the grain and the tip. In the transition domain area in which reversal of the flux occurs, no significant fluxes could be detected. This pattern seems to reflect a gradual, rather than specifically localized, change from one membrane domain to another. Longer tubes (up to 3 mm) were also investigated and again the closed loop at the tip was always detectable (see Fig. 2). Yet two other trends could be also characterized: first, whereas the efflux in the clear zone remained stable, the grain efflux decreased from a certain point on (>2 mm); second, alternate banding of effluxes and influxes arose along the tube in between the tip loop and the grain loop. The size of these alternating bands was not completely regular, and, as in the transition zone in Fig. 1, the magnitude of the fluxes was always one order of magnitude lower than the one driven by the tip and the grain.

A detailed exploration of the tip area in one of these longer tubes (~1.5 mm) is shown in Fig. 2. The plot shows a real-time trace of the vibrating probe, taken with a frequency of 0.5 Hz and an excursion of 10 μm. Under these operating conditions, and with the software used, a datum was generated every 3.3 s. The measuring routine is shown in the inserted cartoon. The probe was first driven to follow the growing apex. As it is shown, the apical domain possesses well-defined, oscillating peaks of proton influx. These oscillations are sustained during long periods of time with sequences up to 30 min being routinely detected, which exhibit stable period and amplitude. In the experi-

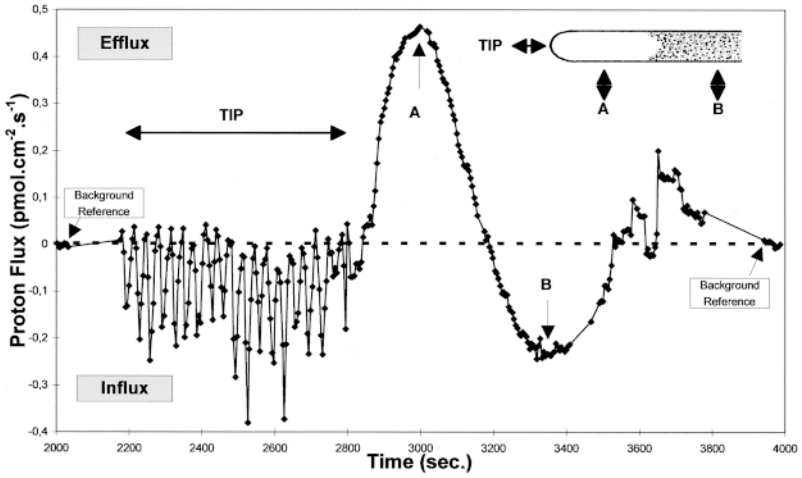

Figure 2. Detailed real-time exploration of the currents around the tip and subtip areas of a tube ~1.0-mm long and grown at pH 6.5. Continuous vibration of the probe at the closest possible point (less than 2 μm) of the growing tip was achieved by very small steps mimicking the tube advance. Under these conditions a sustained oscillatory pattern of the tip proton influx was observed, sometimes during more than an hour, in which the influx could be seen to change from nearly 0 to 0.4 pmol/cm^2/s. From time 2,800 s the direction of the probe vibration was orthogonally changed, and the probe left stationery as the tube was allowed to grow along it (see inset with tube tip). In this circumstance a profile of the proton flux domains underneath the tip was observed without changing the probe position. The physical location of the probe related to the tip is assigned in A and B. As soon as the probe slips out of the tip dome a sharp reversal of the flux occurs and remains as an efflux over a distance that roughly correlates with the extent of the clear zone. Another reversal of the flux is then observed in the rest of the tube, which then evolves to a pattern of small, less defined effluxes. Background reference measurements are included for both directions of probe vibration showing that the bath background fluxes are insignificant in relation to the signal.

ment shown the tip was followed for ~10 min, after which the probe's direction was changed 90° and the subapical domains were mapped. A clear-cut reversal of the current was detected about one tube diameter behind the apical dome, which then peaked in the midpoint of the clear zone (point A in Fig. 2). This specific plot was obtained by halting the probe vibration position, and letting the tube grow past the probe. Therefore, the up and down of the trace reflects the flux topography along the tube, as if the tube had not grown, and the probe was continuously translated along the side of the membrane. At about the point where the clear zone ends and the normal streaming of large organelles is observed, the flux direction reverses again to an influx domain (point B in Fig. 2), which in this example, extends ~100 μm. Along the tube other reversals were then observed, but with much less defined spatial borders, and much lower flux magnitudes. The inserted background references refer to both directions of vibration and clearly show an insignificant noise level, and a very good signal/noise ratio for all measurements plotted in this chart. A spatial representation of a data set similar to this one is shown in Fig. 5 b. It should be stressed that although the lateral fluxes are consistently stable, the vector depicted at the apex is the average of the oscillating flux integrated over 10 min. As will be described, the extracellular proton flux pattern closely matches the adjacent intracellular pattern of pH_c.

Resolution of pH_c Is Strongly Dependent on Probe Concentration

The results above show that significant extracellular fluxes occur, and define specific domains of proton dynamics along the tube. In some instances, especially at low pHs (~5.0), the extracellular expression of these fluxes outside the cell is a measurable gradient which, at the extreme of some apical influx peaks, attained values of ~0.5 pH U over 10 μm. Despite the fact that the intracellular buffering is dramatically different than the weakly buffered germination milieu in which these gradients are formed and detected, it became mandatory to determine if this pattern was in some way expressed inside the tube. We selected BCECF-dextran because it is the most widely used pH probe and has been applied in a number of systems with reliable and reproducible results. Furthermore, the dextran ensures that any pattern that arises is not dependent on organelle sequestration. The first injections were made with a pipette concentration of ~10 mg/ml. When introduced into the cell at this concentration, streaming was abolished at the point of injection and tube growth halted. As the dye diffused along the tube one could observe a progressive inhibition of cytoplasmic streaming with complete blockage after 15–30 min, and no apparent recovery. It followed that at this concentration BCECF-dextran exerted a pronounced deleterious effect, especially on streaming and growth. Using lower concentrations (1 mg/ml) we found that pollen tubes were relatively unaffected in the growth rates or any other structural feature. However, no gradients or hot spots of pH could be observed (Fig. 3 a). Since under these conditions the signal generated was very high, requiring the use of several neutral density filters and exposures of just a few milliseconds, and since at higher concentrations deleterious effects of the probe have been observed, we tried even lower concentrations of BCECF-dextran to fully explore the camera sensitivity and dynamic range. The concentration of the injection solution

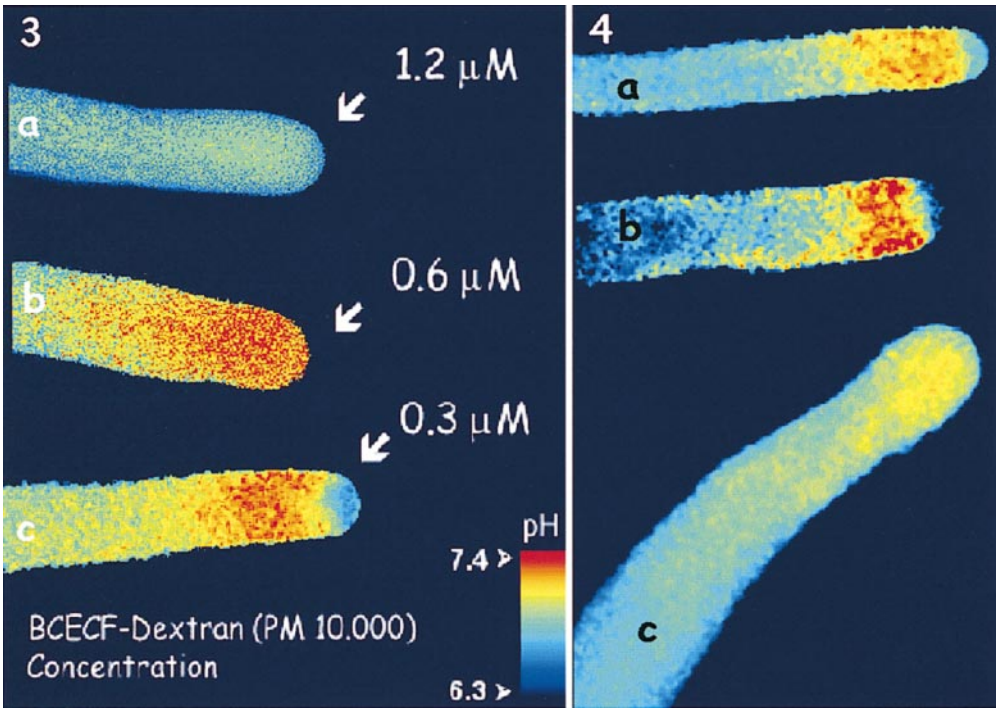

Figure 3. Effect of BCECF-dextran intracellular concentration on the resolution of pH_c. The intracellular concentration was estimated by in vitro/in vivo calibration methods (see Materials and Methods). Only when an estimated concentration of less than 1.0 μM was obtained could some differentiation of the pH_c be observed (b). In tubes injected to final concentrations of less than 0.5 μM, e.g., 0.3 μM (c), a stable spatial pattern of pH_c was always observed, with a distinct alkaline band roughly located over the clear zone area and an acidic tip, often appearing with the shape similar to the inverted cone of vesicles located in close vicinity to the tip. The rest of the tube cytosol was neutral.

Figure 4. Comparison of two growing tubes with different diameters (a and b) and a nongrowing tube (c). Although all growing tubes, regardless of the tube diameter and growth speed, exhibit an alkaline band, only growing tubes show an acidic tip. Note how the alkaline band extends to the apex in nongrowing tubes (c).

was then lowered to 0.7 and then 0.5 mg/ml, again with minimal injection quantities. Below this range, edge artifacts, i.e., optical gradients after ratio provoked by insufficient concentration of the dye on the edges, became evident. Within this range, however, an alkaline gradient became evident in the apical region (Fig. 3 b) and finally, in the optimized conditions for system sensitivity and dynamics, in which there were minimal or no neutral density filters, and in which exposures lasted a few hundred milliseconds, a clear pattern began to emerge that consisted of an alkaline band at the base of the clear zone and an acidic gradient at the extreme apex (Fig. 3 c).

Since the level of the dye seems to be of pivotal importance for understanding the physical basis of this result, we developed a method to estimate its intracellular concentration, which depended on the fluorescence emitted by the pH-independent wavelength (450 nm). The results obtained showed that the threshold concentration for the pattern to be observable is ~0.5 μM, and when the dye concentration is over 1.0 μM, no gradient is detected. Therefore all subsequent experiments were performed in conditions of low dye concentration. The pH_c pattern described above was then observed in all pollen tubes successfully injected and imaged.

Since the use of low dye concentration and long exposures has been systematically reported to potentially give rise to various ratioing artifacts, we undertook a special effort to make sure this did not confound our results. The results obtained are shown in Figs. 5 and 6, which show the raw images corresponding to the tube depicted in Fig. 3 c, without any background subtraction or further manipulation. Of special note is the homogeneous distribution of the dye along the tube, up to the tip, and the complete absence of any detectable sequestration. Fig. 5 c, on the other hand, shows the results of the calibration in pseudocytosol with the same dye concentration (0.3 μM) and the clear response of the dye in the exact same imaging conditions even at these low concentrations. Fig. 5 d brings together (a) transects along the dependent and independent channel images from Fig. 5, a and b; (b) their direct ratio without any background subtraction or thresholding; and (c) the calibration ratio values obtained from Fig. 5 c, using the same imaging and processing parameters. The results show that both dependent and independent traces run parallel until the clear zone, where there is an obvious deviation of the dependent trace. The independent trace stays within the same range up until the tip dome and then quickly decays. The ratio trace reveals a pH_c elevation in

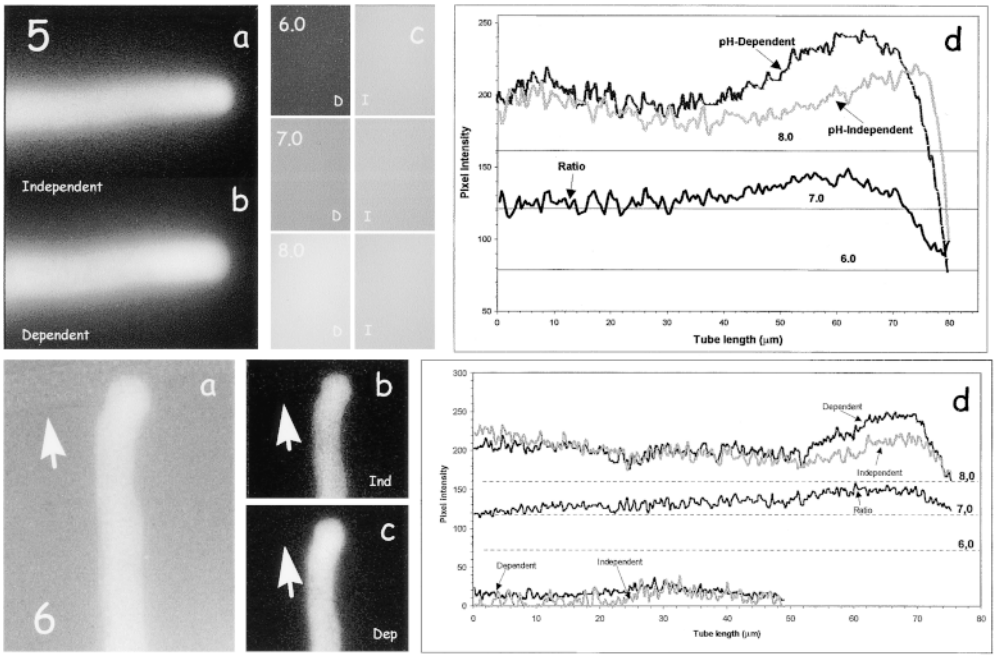

Figure 5. Ratio calculation and calibration from raw images. (a and b) Typical raw images of the pH-independent and the pH-dependent BCECF excitation wavelengths, without background subtraction. (c) In vitro calibration from raw images as collected in exactly the same filter and integration conditions. The left half (D) represents the pH-dependent excitation wavelength and the right half (I) represents the pH-independent excitation wavelength. Calibrations were made in pseudocytosol medium (see Materials and Methods) contained 0.35 μM BCECF-dextran, and an approximate thickness of 15 μm between slide and coverslip (as calculated from the volume applied). Note that the pixel intensity in the independent channel is similar in the three images and similar to the pixel intensity along the midtransect of the pollen tube independent wavelength image. (d) Ratio values as calculated directly from the raw images (a, b, and c) without background subtraction. The lines represent the pixel profiles along the midsection of the tube and their ratio (dependent/independent × 130). The horizontal lines represent the calibration ratio value calculated by averaging the pixel intensity of square boxes with 2,000 μm^2, as in c.

Figure 6. Image of a growing BCECF-loaded tube that impacts an unloaded tube (arrow). (a) Mixed fluorescence/transmitted light image shows the relative position of the two tubes. (b) The fluorescence collected in the pH-independent channel and (c) in the pH-dependent channel. The graph plotted in d summarizes the mid line scans of both b and c, their respective ratio (dependent/independent × 130) and the calibration values collected under the same imaging conditions (see Fig. 5). The two bottom traces correspond to mid line scans along the unloaded tube (arrows) from the fluorescence images b and c. The slight elevation at 30 μm corresponds to the area where the tip of the loaded tube abuts the unloaded tube. The mean pixel intensity plotted in the upper and lower traces can be taken as an indirect measure of the signal/noise ratio of the system used, namely, ~10-fold. An acidic tip in the loaded tube is not seen because the tube slowed markedly in growth after striking the unloaded tube.

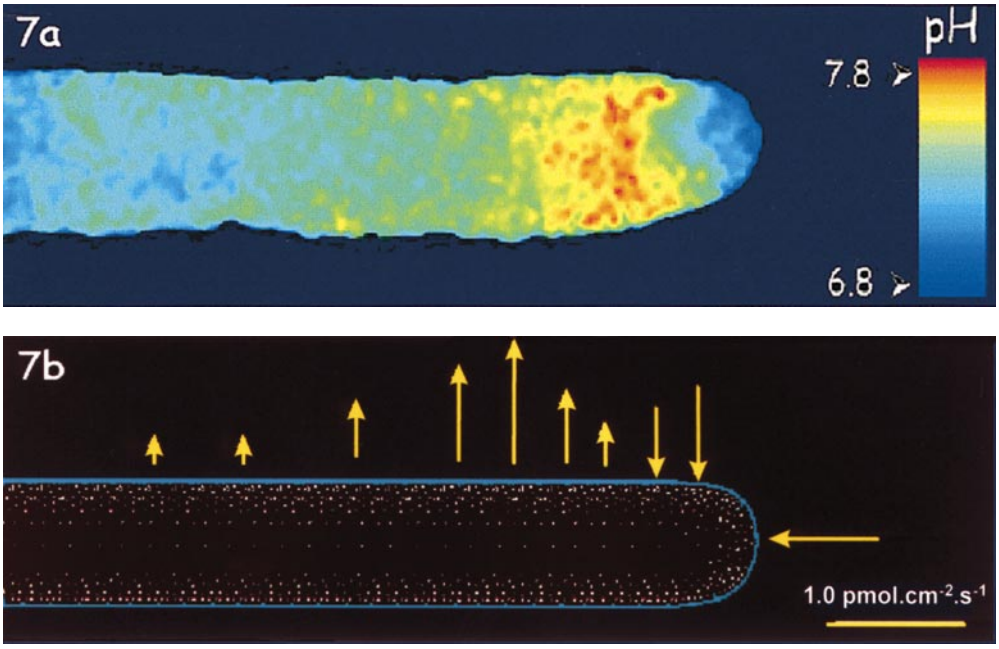

Figure 7. Comparison of the pH_c (Fig. 7 a) and the extracellular proton fluxes (Fig. 7 b) in two tubes with matching sizes, growth rates, length, and extracellular pH. A close correlation is observable between the cytosolic alkaline band and the patterns of proton efflux, in which both roughly correspond to the domain occupied by the clear zone. Again the tip inverted cone is clearly visible in the pH_c picture. Although these patterns were obtained in different tubes, they show a close correlation, suggesting that the elevation of pH_c in the clear zone may correspond (at least partly) to an active proton efflux in the same area.

the beginning of the clear zone, reaching a plateau ~7.5, which lasts for ~20 μm and a decrease within 10 μm to ~6.5. Fig. 6 explores the signal to noise ratio in these working conditions. The image shows two tubes, in which one has a typical dye load, while the other is nonloaded; both tubes are depicted in a combined low-light transmitted/fluorescence image (Fig. 6 a). The raw images (Fig. 6, b and c) indicate almost no detectable light in the area of the nonloaded tube. The traces are brought together in Fig. 6 d and display a signal to noise ratio that is ~10-fold. Although an alkaline band is visible, there is no acidic tip since this tube had been inhibited in growth after impacting the nonloaded tube.

The correlation of the intracellular and extracellular patterns was then established, as shown in Fig. 7. Simultaneous imaging and vibrating probe analysis, due to technical limitations, has not been possible. Therefore, correlations were made through the comparison of two different pollen tubes, which were chosen with similar growing and structural characteristics (growth medium, length, growth rate, tube diameter, and clear zone extension). Six tubes were compared with very similar characteristics. A correlation of the one depicted in Fig. 7 revealed that the alkaline band corresponded generally to the proton efflux domain.

Pollen Tubes Have a Constitutive Alkaline Band and an Acidic Tip That Is Dependent on Growth

Given the observations of alkaline and acidic domains, we addressed the question whether or not this intracellular pattern was related to the growth, or even implicated in its regulation. We sought to observe tubes with different growth rates (or fully stopped) and different tube diameters. Fig. 4 shows two growing tubes with different diameters (12 and 15 μm) and different growth rates (tube a growing at 18 μm/min and tube b at 7 μm/min). They both have a distinct alkaline band, but the acidic tip of the slowly growing tube is smaller. A fully stopped tube (Fig. 4 c) also shows the alkaline band, but the acidic tip is totally absent. It thus seems that although the alkaline band is constitutive, the acidic tip is dependent on growth. These results were confirmed through a stop-and-go experiment (see Fig. 9) in which tube growth was halted by gentle addition of medium with increased osmolarity, followed by growth reinitiation when returned to normal medium. Growth recovery occurs within 10–20 min and could be followed to the moment when the newly formed tube protruded from the tip. This sequence (see Fig. 9) shows the formation of the slightly acidic domain, which will constitute the apical cytosol.

Since most of the tubes over 800 μm display oscillatory proton influxes at the tip and oscillatory growth rates, we then tried to follow the variations of pH during growth. A typical result is displayed in Fig. 8. Two features emerge from these sequences: first, there is a periodic change in pH_c, especially expressed in the alkaline band, and second, the shape and position of the acidic tip also changes, from plano-convex when the alkaline band pH is higher, to an inverted, or bi-convex cone when the pH decreases (see figure legend for details). Furthermore, in the final two frames, where the tube bends, the acidic tip is also asymmetric with the lowest pH region corresponding to the direction of pollen tube elongation. The deformation of the acidic tip would then be consistent with a flux of protons entering through the extreme apex, which would lower pH_c in the alkaline band. Further analysis of this correlation was assayed and the variations of the alkaline band pH were plotted together with the growth rate (see Fig. 12). The use of diluted probe solutions renders the injected cells susceptible to photobleaching, restricting the time resolution to 15–20 s. The sequence plotted had an interval of 16.5 s between consecutive frames. Thus, although precise correlation is difficult, the global trend shows that when pH_c increases in the alkaline band, the growth rates decrease, and conversely, when pH_c de-

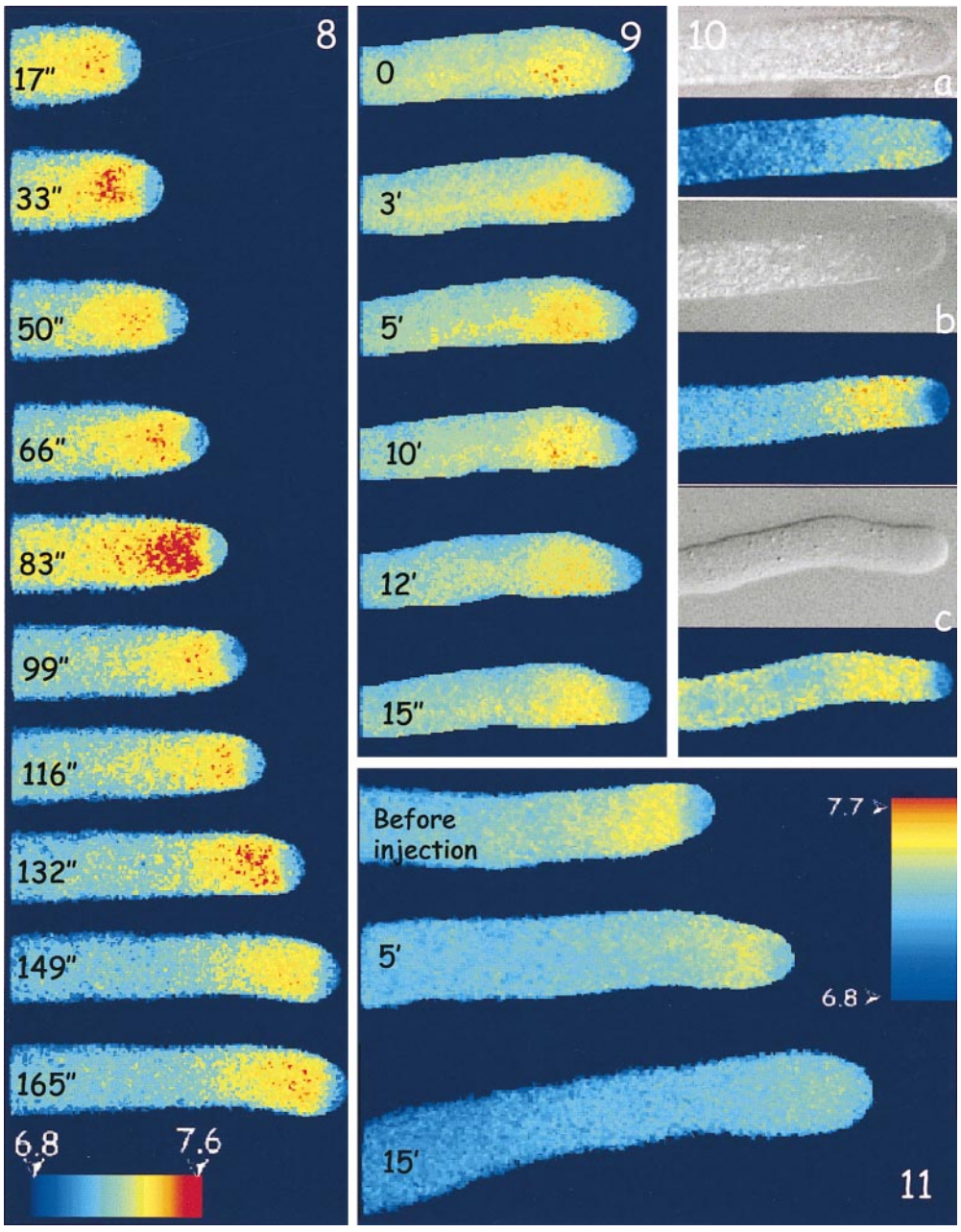

Figure 8. pH_c time sequence of a growing pollen tube. Numbers on top of the tubes are seconds from the beginning of the sequence. The mean interval between frames is 16.5 s. An elevation of pH_c in the alkaline band is clearly visible at times 33, 83, and 132 s, reflecting possible oscillations of pH_c in this area of the cytosol. The images also suggest some variations of the acidic tip, but these ones proved to be more difficult to quantify. Also visible is the change of shape of the acidic tip. At times 17, 50, and 132 s it has a biconvex shape. However, at times 33, 83, and 116 s the shape changes to plano-convex, and at time 66 s it shows the typical inverted cone configuration. Frames at 99, 149, and 165 s show asymmetric acidic tips which, in the later two cases, follow the change in growth direction.

Figure 9. Typical result of an experiment in which growth was arrested with an osmotic shock and allowed to restart after replacement of the normal medium. Numbers represent time in minutes from the beginning of the sequence. The sequence shows the moment where growth restarts (third frame, time 5 min). The alkaline band is slightly asymmetric, with the higher values closer to the half tube from which the new tip is going to protrude. Before this happens no acidic tip is clearly discernible. Yet, when the new tip arises (fourth and fifth frames, 10–12 min.) it defines a slightly acidic area of cytosol. The alkaline band then follows the acidic tip into the newly formed tube, which is easy to spot due to its smaller diameter (sixth frame, 15 min) (refer to Fig. 11 for calibration wedge).

Figure 10. Comparison of the clear zone extension and the cytosol alkaline band. Three tubes with increasing lengths of their clear zone are shown in transmitted light (a–c) and the respective image for pH_c (a′ to c′). Even though all tubes are growing with similar growth rates, they possess very different clear zones. Tip a belonged to a very elongated tube (>3.0 mm) and has a clear zone restricted to the terminal 15 μm, behind which the streaming of large organelles was vigorous. Correspondingly, the alkaline band was more restricted but the acidic tip appeared normal (compare with Fig. 5 a). Tube b represents the more typical situation, with a clear zone of ~50 μm. In these tubes the alkaline band is very well defined, and its length extends to about the point where the streaming of the large organelles terminates. More rarely, tubes with very extended clear zones (sometimes over 200 μm) were also observed, as in c. In this case the alkaline band is also very well defined, but several hot spots of pH elevation occur along the tube membrane (c′). These elevated regions fade where the streaming terminates. Note that in the three cases shown, the acidic tip remains more or less equivalent in size and magnitude (refer to Fig. 11 for calibration wedge).

Figure 11. Effect of buffer injection on pH_c of a growing pollen tube. A standard growing tube was first injected with BCECF-dextran and imaged (first frame). As expected, it shows the alkaline band and the acidic tip. It was then further injected with Hepes (see Materials and Methods) and followed for determination of the buffer effect. The second frame was obtained immediately after needle withdrawal, and ~5 min after the buffer injection. Growth rate was nearly the same but the alkaline band seems to have been narrowed. 15 min after injection (third frame), the tube continued to grow, although at a lower rate (from 15.0 to 9.0 μm/min) but the alkaline band is now either absent or beyond the resolution limit of the imaging system.

creases (or in other words, proton concentration increases) the growth rates increase. Taken together, the results are globally consistent with the model of a constitutive alkaline band that is, at least partly, generated by proton extrusion, and a slightly acidic tip that is, at least partly, dependent upon localized proton influx. Moreover, pollen tube elongation appears to be correlated with the concentration of protons in the extreme apex.

The Alkaline Band Is Spatially Correlated with the Apical Clear Zone

It became evident from the first experiments that there was a general agreement between the size and position of the clear zone, the proton efflux domain, and the alkaline band. The clear zone corresponds to the tip portion of the cytoplasm in which streaming does not occur and large organelles are excluded. The molecular basis for this polar behavior seems to be related to the disruption or reorganization of the actin cables that drive streaming (Miller et al., 1996). For unknown reasons, the clear zone, although having a typical length for a given species, displays a natural variation in length. These variations do not correlate with growth rates or tube diameter, and during these studies clear zones ranging from 15 to more than 300 μm were observed. Some of these extreme examples were injected with BCECF-dextran in order to establish the possible spatial correlation of the alkaline band and the clear zone. Three typical results are shown in Fig. 10. A very short clear zone (a) corresponds to a much more vaguely defined alkaline band when compared with the standard 50-μm clear zone (b). Likewise a tube with a very long clear zone also shows a very extended alkaline band with several hotspots along the membrane (c).

Buffer Injection Destroys the Gradient but Does Not Inhibit Growth

One of the central issues in all pH_c results presented so far concerns the effect of the dye/buffer concentration on the visualization of the gradient. Since the probe itself functions as a buffer, it was hypothesized that higher concentration of the dye would function as a mobile buffer and disrupt the gradient beyond the resolution of the imaging system. To test this hypothesis, tubes were injected under standard conditions that permitted reproducible resolution of the pattern shown in Fig. 7 a and were then injected with Hepes buffer. A typical result is shown in Fig. 11. As soon as the buffer starts to diffuse (Fig. 11 b) the alkaline band starts to fade and 15 min after injection, it is hardly discernible. Although the growth rate was reduced from 15 to 9 μm/min, pollen tubes continued to grow under conditions in which a pH_c gradient is no longer detected. Injection of higher quantities of Hepes irreversibly halted growth and, in extreme cases, completely abolished cytoplasmic streaming.

Discussion

The Existence of a pH_c Gradient in Growing Pollen Tubes

Using two complimentary methods we provide evidence that growing pollen tubes possess a pH gradient. The extreme apex is acidic whereas a region corresponding to the base of the clear zone displays an alkaline band. These conclusions derive from the observations that (a) depict directly the existence of a localized gradient, (b) associate the characteristics of this gradient with either growth (acidic tip) or a structural feature (alkaline band), and (c) establish complimentary profiles between extracellular proton fluxes and intracellular proton distribution.

Although we cannot exclude the possibility that our results are species specific, or occur only in long, oscillating pollen tubes, they could explain the failure of the previous reports (Parton et al., 1997; Fricker et al., 1997; Messerli and Robinson, 1998) to detect the apical pH_c gradient. In brief, we suggest that when the indicator dye is elevated to 1 μM or more it becomes sufficiently active as a shuttle buffer to dissipate local pH gradients. Not only do the studies on the calibration of the dye concentration support this claim, but the additional experiments in which we injected differing amounts of a pH buffer reveal that the gradient can be predictably modified, without necessarily inhibiting pollen tube elongation. Thus we have been able to reproduce the results of the other published reports (Fig. 3). However, by producing ratio images at low dye concentrations in a system with optimized sensitivity, we were able to resolve a pH_c gradient in lily pollen tubes.

Although the confocal microscope is a powerful observational instrument (Hepler and Gunning, 1998), it may not be ideally suited for ratiometric ion analysis, due in part to the relatively high level of excitation and/or high dye concentration needed to form a good quality image in a single thin optical section. Indeed, as pointed out by Opas (1997), "Confocal microscopy, in its present incarnation, is not best suited for multiwavelength detection of

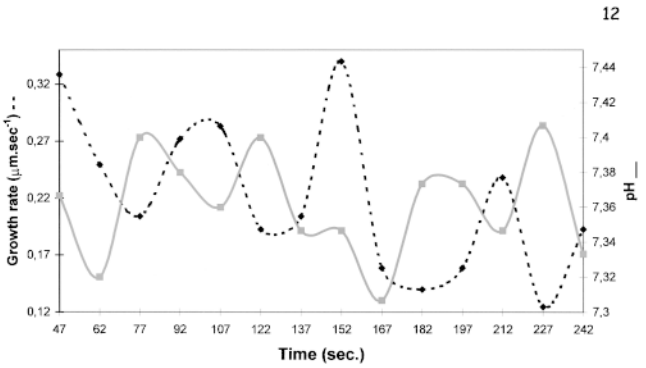

Figure 12. Correlation between pH_c oscillations in the alkaline band and growth rate on the same tube. At the low probe intracellular concentrations used, the time interval (25 s) shown represents the best possible compromise between fading and time-resolution. Although not allowing precise correlation, oscillatory variations (i.e., with at least three full cycles) of pH_c in the alkaline band were detected, with periods ranging from 25 to 55 s. In most of these the correlation of pH_c at the alkaline band and the growth rate showed the trend depicted in this plot, i.e., when growth goes up, the pH goes down (or, in other words, proton concentration goes up). At this time resolution, however, a significant portion of the wave function is lost and precise correlation is not possible.

weak fluorescent signals and their fast changes. If such signals are to be detected a dedicated wide-field system should be employed." In the present study we have specifically used a wide-field imaging system enabling us to work at dye concentrations, at least one order of magnitude below most of the estimates of intracellular BCECF or seminapthorhodafluor (SNARF-1) used by others (Fricker et al., 1993, 1994, 1997; Parton et al., 1997; Messerli and Robinson, 1998). One danger of working at low dye concentrations is the possible "edge-artifact," i.e., the possibility of creating false gradients by insufficient dye concentration in the edges of a curved surface, where the optical path is shorter. We are, however, confident that this has not compromised our results since we found this threshold to be below 0.1 μM. Furthermore, if such an aberration were present, it would not produce the fine characteristics of the acidic tip shown for the stop-and-go experiment (Fig. 9) or in the temporal sequences (Fig. 8), where the pollen tube changes shape according to the growth behavior, and it would not be affected by the injection of a nonfluorescent pH buffer (Fig. 11). Also the detailed analysis of the raw images (Figs. 5 and 6) shows no evidence of low-light artifacts or insufficient signal to noise ratio. Indeed, the ratio lines, numerically derived directly from transects of the raw images, produce the exact same pH_c profile, and further reveal that the signal is ~10-fold above the background fluorescence.

The Membrane Basis of the Gradient

Although the image of the acidic domain in the pollen tube apex and alkaline band at the base of the clear zone make it appear as if these ionic distributions are expressed throughout the thickness of the pollen tube, we think instead that they are manifest only close to the plasma membrane. It must be stressed that these ratiometric images are not optical sections, but are projections of virtually the entire tube volume onto a single image plane. Thus the alkaline band in reality may be a cortical ring or torus, with maximal expression at the inner surface of the plasma membrane. Similarly the acidic domain in the pollen tube apex is likely to be a hollow cone dominated by the intense proton influx at the plasma membrane. This explanation would account for the observed fact that growth is not abolished in the absence of a detectable gradient. It seems quite likely, under conditions of elevated dye concentration, that the gradient is still present but because it is closely situated next to the plasma membrane, where its action may lay, it is below the resolution limit of the microscope systems used thus far. In support of this contention we refer to the study of Stern (1992) on the local $[Ca^{2+}]$ in the vicinity of a pore, which shows that the application of an exogenous Ca^{2+}-buffer steepens the existing gradient, rather than reducing its high point. We suggest that a similar phenomenon affects the local pH_c gradient in response to a pH dye or buffer, in which the gradient, although steep in magnitude, is spatially restricted to a zone 10–20 nm from the plasma membrane. Since, even under optimal conditions, it is unlikely that resolutions under 200 nm are achieved, it can readily be appreciated that the microscope would be incapable of detecting a gradient of molecular dimensions appressed to a membrane. Indeed, in the wide-field system used in this study, there has been some sacrifice of spatial resolution to satisfy light-gathering needs. Thus, each pixel on the CCD represents 0.29 μm, whereas the Nyquist requirements for maximal spatial resolution demand sampling at 0.07 μm (Pawley, 1995; Hepler and Gunning, 1998). We conclude, therefore, that under conditions of limited buffering, which permit growth to continue, a functional pH gradient might exist as a consequence of membrane flux anisotropies, but that its restricted spatial dimensions render it undetectable in currently used optical systems.

The question thus remains how protons are transported in to and out from the apical region. Proton entry, accounting for the apical acidic domain, is an exergonic reaction from a medium of high proton concentration, pH 5.5–6.0, relative to the cytoplasm (bulk ~pH 7.0). Although specific proton channels have not yet been described there is evidence that other cationic channels, notably stretch-activated Ca^{2+} channels, which have been postulated to be active in the pollen tube apex (Obermeyer et al., 1991; Malhó et al., 1995; Feijó et al., 1995; Pierson et al., 1996), are known to be relatively nonspecific and may allow entry of potassium and protons (Yang and Sachs, 1989). Although Ca^{2+} and H^+ distribution is not exactly identical in the pollen tube tip there is substantial similarity arguing in support of a similar mechanism of entry.

Proton efflux is most likely driven by the ubiquitous H^+-ATPase that is responsible for proton extrusion activity in the plasma membrane of plant cells (Sze, 1985; Al-Awqati, 1986; Briskin and Hanson, 1992), including pollen (Feijó et al., 1995). Although most studies indicate that the pollen grain exhibits high H^+-ATPase activity, there is some controversy concerning the location of this activity in the tip domain (Feijó et al., 1992; Obermeyer et al., 1992). For example, a monoclonal antibody against the 100 kD H^+-ATPase of maize plasma membranes shows no labeling (Obermeyer et al., 1992), whereas clear ATPase activity, compatible with a H^+-ATPase, was detected by enzyme cytochemistry in both *Agapanthus umbellatus* (Feijó et al., 1992) and *Ophrys lutea* (Feijó et al., 1994a), which is fully compatible with the extracellular fluxes described herein. Since the ionic dependencies of the tip H^+-ATPase were slightly different from those in the pollen grain, we may hypothesize that they represent a different protein, which could account for the differences in immunolabeling (Obermeyer et al., 1992). In attempting to account for the polarized location of this pump, one possibility is that it is introduced into the apex during vesicle fusion. However, because of the high $[Ca^{2+}]$ at the extreme apex, the activity of the H^+-ATPase would be inhibited, as described in other systems (Kinoshita et al., 1995; Lino et al., 1998), whereas back from the apex, where the $[Ca^{2+}]$ is at a basal level, the pump would exert maximal activity, an idea that is consistent with our vibrating probe data.

Mechanisms That Contribute to the Formation of a pH_c Gradient in Growing Pollen Tubes: From Diffusion to Reaction-Diffusion

Given that growing pollen tubes possesses a substantial pH_c gradient, it becomes a question how this is generated, especially since pH_c is known to be homeostatically con-

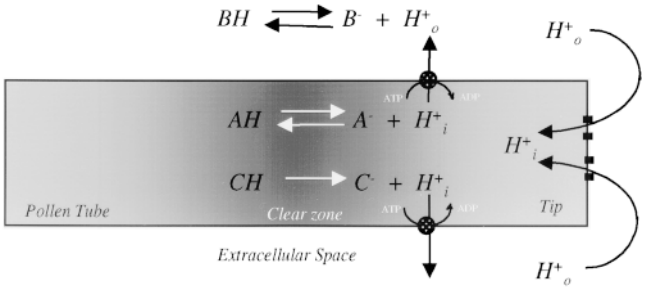

Figure 13. A model for proton gradients in pollen tubes. The geometry of the tube has been simplified to a two-dimensional rectangular section and the pivotal assumptions have been based on the pattern described for extracellular fluxes. A and B represent the intracellular and extracellular buffers, and C the metabolic irreversible proton formation (see text and also Appendix for mathematical details).

trolled within close tolerances. We initially attempted to apply a linear diffusion model that relied on three concepts, namely: (a) the cytosolic buffering capacity; (b) the relative mobility of protons and buffers; and (c) the fluxes needed to overcome pH_c buffering capacity. Although used successfully in an analysis of pH in extracted axoplasm in a artificial chamber (Al-Baldawi and Abercrombie, 1992), the conditions are clearly inadequate for the growing pollen tube where there are marked asymmetries, even spatial separation, in the distribution of pumps and channels, which will create proton anisotropies. In addition, buffering capacity in the pollen tube is likely to be unevenly distributed with that in the clear zone being less than the shank since most of the organelles with active metabolic pathways and immobile buffering systems, e.g., vacuoles (Smith and Reid, 1991; Frohnmeyer et al., 1998), are excluded from the clear zone. When these issues are considered together with the realization that the concepts of linear diffusion fail to acknowledge that intracellular buffers are themselves the product of metabolic reactions that yield or consume H^+, and that buffering capacity depends on pH_c itself (Ravesloot, 1998), it becomes necessary to introduce features of nonlinearity.

A more realistic model is one typified by a reaction-diffusion system that incorporates kinetic terms related to metabolism and transport processes, and diffusion terms imposed by the differential localization of membrane fluxes; when taken together these factors can amplify anisotropy in ion distribution, and possibly account for the formation of pH gradients in pollen tubes. We summarize our thinking in Fig. 13 where, for the sake of simplicity we reduce the problem to a two-dimensional space and simplify the geometry of the pollen tube to a rectangular shape. The model considers two compartments, the intracellular and extracellular spaces, separated by an interface with heterogeneous permeability properties. In the tip, proton influx exhibits saturation kinetics imposed by the transport limitations of the specific carriers; we suggest that within this area the spatial distribution of ionic channels is uniform. We also define nonapical areas rich in active ATPase systems that actively extrude protons. We stress that these biological conjectures are supported by the results obtained with proton selective vibrating electrodes reported herein.

The model, depicted graphically in Fig 13 and mathematically in the Appendix, draws attention to three critical factors in the global control of proton flux, as follows: (a) intracellular buffering associated with the cellular regulation of pH; (b) extracellular buffering; and (c) fluxes between the intracellular and extracellular compartments. Thus, in accordance with a typical reaction-diffusion system, the model incorporates kinetic terms related to metabolism and transport processes, and diffusion terms imposed by the differential localization of membrane fluxes. Although we cannot offer a numerical resolution of the model because we lack the exact buffering and apparent proton diffusion coefficients in pollen tubes, nevertheless we note that the system has the necessary conditions to support the spontaneous emergence of stable spatial patterns (Turing, 1952; Murray, 1993; Gray and Scott, 1994). In addition, the equations provide a means to account for transient neutralization of a pH gradient through the addition of weak acids or bases. The plausibility of the model gains support from previous observations showing that pollen tubes possess a calcium gradient (Holdaway-Clarke et al., 1997; Messerli and Robinson, 1997), which, in addition to the proton gradient demonstrated herein, oscillates in concert with periodic changes in the growth rate.

Cytological Consequences of the Gradient: pH_c as a Spatial Organizer in Apical Growth?

There are many processes within the pollen tube that could be affected by localized pH domains; we will direct attention to only a few. First, given the relationship between acidification and the events of exocytosis and endocytosis, it would seem likely that the high levels of protons at the pollen tube apex would be involved. Exocytosis, which is essential for pollen tube elongation, involves the delivery of new membrane to the existing plasma membrane and material to the expanding wall. In certain systems acidification promotes the process; for example, in turtle bladder low pH facilitates the exocytosis of membrane containing H^+-ATPase activity (Gluck et al., 1982). Although many details need to be experimentally resolved, the close spatial correlation between the locus of secretory events and the pH_c gradient support the contention that the latter contributes to the former.

The cytoskeleton is another target for the regulation by pH_c (Yonezawa et al., 1985; Suprenant, 1991; Andersland and Parthasarathy, 1993; Edmonds et al., 1995) with particular attention being directed towards actin microfilaments. It is well known that an actomyosin system, which generates cytoplasmic streaming and transports the vesicles to the apical region, is essential for pollen tube growth. However, the streaming lanes do not penetrate the apical clear zone, but instead terminate at its base. Studies on the structure and distribution of actin microfilaments, in close agreement, show that the prominent cables also do not extend into the clear zone but become diffusely organized in this region (Miller et al., 1996; Kost et al., 1998). With the realization, as shown herein, that this interface is also the locus of the alkaline band, it becomes attractive to consider the possible interaction between pH_c levels, and actin organization and dynamics. There are many actin-binding proteins, of which some show sensitiv-

ity to pH_c. We briefly mention two, elongating factor-1α (EF-1α) and cofilin/actin-depolymerizing factor (ADF), both of which facilitate the remodeling of actin gels and networks at slightly alkaline pH levels (7.2–7.3) (Yonezawa et al., 1985; Moon and Drubin, 1995; Murray et al., 1996). It is further important to note that members of the cofilin/ADF family exist in pollen, including both lily (Kim et al., 1993) and maize (Lopez et al., 1996), where pollen-specific forms of ADF have been identified. Cytochemical studies on ADF in root hairs, another tip growing cell, reveal that the protein is localized at the apex, where actin remodeling is thought to occur (Jiang et al., 1997). Although direct observation is needed, it nevertheless seems plausible that cofilin/ADF might reside near the region of the alkaline band in pollen tube where it participates in F-actin turnover and growth.

Finally, it is pertinent to consider the basal and apical closed loops of proton currents (or proton short circuits) and their possible role in pollen tube growth. It has been argued that they are the result of underlying local cellular process and that both the external and internal paths lack a functional significance (Harold and Caldwell, 1990). Yet it is possible that these current loops could generate either an electrostatic field driving force or a trigger (Jaffe, 1977; Nuccitelli, 1983; DeLoof, 1986) that influences, for example, the directed flow of vesicles to the apex. Here it should be noted that pollen tubes, contrary to other systems such as root hairs (Bibikova et al., 1997), do not display an endogenous polarity, but may readily change the direction of growth in response to a number of stimuli (Malhó and Trewavas, 1996). The apically localized current loop of the pollen tube may be a property that allows the cell to perceive and respond to extracellular signals. Agents or conditions that interact with the loop on the outside could change its characteristics in ways that produce modifications in the alkaline band, which in turn alter F-actin organization and/or vesicle secretion, and thus cause the pollen tube to redirect its growth.

Appendix

To help understand the control of protons in both intracellular and extracellular compartments we define two buffer systems with different physicochemical properties as follows:

$$AH \underset{k_{-1}}{\overset{k_1}{\rightleftarrows}} H_i^+ + A^- \tag{1a}$$

$$BH \underset{k_{-2}}{\overset{k_2}{\rightleftarrows}} H_o^+ + B^- \tag{1b}$$

where AH and A^- represent the concentrations of a weak acid and its conjugate base. In buffering conditions, i.e., at instantaneous equilibrium, the proton concentration is given by:

$$H_i^+ = k_{a1}\frac{AH}{A^-} \tag{2a}$$

$$H_i^+ = k_{a2}\frac{BH}{B^-} \tag{2b}$$

where k_a represents the ionization constants of weak acids. Through the application of the Henderson-Hasselbalch equation (Christian, 1986), the numerical results can be converted directly to the pH scale.

The transmembrane transport systems, due to rate limitations, are represented by saturation functions that depend on the respective proton concentrations. In a first approximation we consider functions in the form of the Michaelis-Menten equation (Cornish-Bowden, 1995):

$$f(H_i^+) = \frac{V_i H_i^+}{K_i + H_i^+} \tag{3a}$$

$$g(H_o^+) = \frac{V_o H_o^+}{K_o + H_o^+} \tag{3b}$$

where V and K represent the apparent kinetic parameters related with the maximum velocity and affinity for proton transport, respectively.

Additionally, and as a consequence of the irreversible metabolic activity, an intracellular homogeneous production of H^+ (Fig. 13) is also considered, as indicated below:

$$CH \overset{k_3}{\rightarrow} H_i^+ + C^-. \tag{4}$$

Applying the mass action law to the biochemical reaction (Eq. 4) above yields an autonomous differential equation of the form:

$$\frac{dH_i^+}{dt} = k_3 CH. \tag{5}$$

Merging these physical and chemical conjectures yields the following partial differential equations:

$H_i^+ \approx$ intracellular buffer effect + metabolic proton production – proton efflux + proton influx + proton diffusion

$$\frac{\partial H_i^+}{\partial t} = k_{a1}\frac{AH}{A^-} + k_3 CH - f(H_i^+) + g(H_o^+) + D_{H_i^+}\nabla^2 H_i^+ \tag{6a}$$

$H_e^+ \approx$ extracellular buffer effect – proton influx + proton efflux + proton diffusion

$$\frac{\partial H_o^+}{\partial t} = k_{a2}\frac{BH}{B^-} - g(H_o^+) + f(H_i^+) + D_{H_o^+}\nabla^2 H_o^+. \tag{6b}$$

These equations include both kinetic and diffusion terms, where D_{H^+} represents the apparent diffusion coefficients in two media, and $\nabla^2 H^+$ is a condensed representation of Fick's second law denoted by the Laplace operator. We also assume that buffer variables are constant and have a homogeneous spatial distribution within this compartment. These equations represent a reaction-diffusion system capable of supporting a stable spatial pattern.

We thank A. Shipley (Applicable Electronics, Forestdale, MA) for generous donation of equipment to the Vibrating Probe Facility (University of Massachusetts, Amherst, MA) and R. Beckwith and M. Johnson (University of Massachusetts, Amherst, MA) for help in growing the plants. We also thank T. Holdaway-Clarke (University of Massachusetts, Amherst, MA) for helpful discussions.

J.A. Feijó received personal fellowships from the Fulbright Founda-

tion, Luso-American Foundation for Development, Calouste Gulbenkian Foundation, and Junta Nacional de Investigação Cientifica e Tecnologica. This project was supported by a grant from the National Science Foundation (MCB-96-01087) to P.K. Hepler.

Received for publication 29 July 1998 and in revised form 21 December 1998.

References

Al-Awqati, Q. 1986. Proton-translocating ATPases. *Annu. Rev. Cell Biol.* 2:179–199.

Al-Baldawi, N., and R.F. Abercrombie. 1992. Cytoplasmic hydrogen ion diffusion coefficient. *Biophys. J.* 61:1470–1479.

Andersland, J.M., and M.V. Parthasarathy. 1993. Conditions affecting depolymerization of actin in plant homogenates. *J. Cell Sci.* 104:1273–1279.

Bachewich, C.L., and I.B. Heath. 1997. The cytoplasmic pH influences hyphal growth and cytoskeleton-related organization. *Fungal Gen. Biol.* 21:76–91.

Bibikova, T.N., A. Zhigilei, and S. Gilroy. 1997. Root hair growth in *Arabidopsis thaliana* is directed by calcium and an endogenous polarity. *Planta.* 203: 495–505.

Blowers, D.P., and A.J. Trewavas. 1989. Second messengers: their existence and relationship to protein kinases. *In* Second Messengers in Plant Growth and Development. W. Boss and D.J. Moore, editors. Alan R. Liss, New York. 1–28.

Bright, G.R., J.E. Whitaker, R.P. Haugland, and D.L. Taylor. 1989. Heterogeneity of the changes in cytoplasmic pH upon serum stimulation of quiescent fibroblasts. *J. Cell Physiol.* 141:410–419.

Briskin, D.P., and J.B. Hanson. 1992. How does the plant plasma membrane H^+-ATPase pump protons? *J. Exp. Bot.* 43:269–289.

Christian, G.D. 1986. Analytical Chemistry. John Wiley, New York. 648 pp.

Cornish-Bowden, A. 1995. Fundamentals of Enzyme Kinetics. Portland Press, London, UK. 343 pp.

Cosson, P., I. de Curtis, J. Pouyssegur, G. Griffiths, and J. Davoust. 1989. Low cytoplasmic pH inhibits endocytosis and transport from the trans-Golgi network to the cell surface. *J. Cell Biol.* 108:377–387.

DeLoof, A. 1986. The electrical dimension of cells: the cell as a miniature electrophoresis chamber. *Inter. Rev. Cytol.* 104:251–352.

Dixon, G.K., C. Brownlee, and M.J. Merrett. 1989. Measurement of internal pH in the coccolitophore *Emiliana huxleyi* using 2′,7′-bis-2-carboxyethyl-5 and -6 carboxyfluorescein acetoxymethylester and digital imaging microscopy. *Planta*. 178:443–449.

Dube, F., L. Dufresne, L. Coutu, and G. Clotteau. 1991. Protein phosphorylation during activation of surf clam oocytes. *Dev. Biol.* 146:473–482.

Edmonds, B.T., J. Murray, and J. Condeelis. 1995. pH regulation of the F-actin binding properties of *Dictyostelium* elongation factor 1 alpha. *J. Biol. Chem.* 270:15222–15230.

Feijó, J.A., R.G. Martinho, and M.S. Pais. 1994a. Pollen germination and tube growth in massulated orchids: structural aspects, ATPase distribution and cytoskeleton organization in *Ophrys lutea* Cav. *In* Frontiers in Sexual Plant Reproduction. E. Heberle-Bors, M. Hesse, and O. Vicente, editors. University of Vienna, Austria. 58.

Feijó, J.A., A.M. Shipley, and L.F. Jaffe. 1994b. Spatial and temporal patterns of electric and ionic currents around *in vitro* germinating pollen of lily. *In* Frontiers in Sexual Plant Reproduction. E. Heberle-Bors, M. Hesse, and O. Vicente, editors. University of Vienna, Austria. 40.

Feijó, J.A., R. Malhó, and M.S. Pais. 1992. A cytochemical study on the role of ATPases during pollen germination in *Agapanthus umbellatus*. *Sex. Plant Reprod.* 5:138–145.

Feijó, J.A., R.M. Malhó, and G. Obermeyer. 1995. Ion dynamics and its possible role during in vitro germination and tube growth. *Protoplasma.* 187:155–167.

Felle, H. 1988a. Cytoplasmic free calcium in *Riccia fluitans* L. and *Zea mays* L.: interaction of Ca^{2+} and pH? *Planta*. 176:248–255.

Felle, H. 1988b. Short-term pH regulation in plants. *Physiol. Plantarum*. 74: 583–591.

Felle, H. 1989. pH as a second messenger. *In* Second Messengers in Plant Growth Development. W.F. Boss and D.J. Morré, editors. Alan R. Liss, New York. 145–166.

Fricker, M.D., N.S. White, and G. Obermeyer. 1997. pH gradients are not associated with tip growth in pollen tubes of *Lilium longiflorum*. *J. Cell Sci.* 110: 1729–1740.

Fricker, M.D., M.R. Blatt, and N.S. White. 1993. Confocal fluorescence ratio imaging of pH in plant cells. *In* Biotechnology Applications of Microinjection, Microscopic Imaging and Fluorescence. P.H. Bach, C.H. Reynolds, J.M. Clark, J. Mottley, and P.L. Poole, editors. Plenum Press, New York. 153–163.

Fricker, M.D., N.S. White, G. Thiel, P. Millner, and M.R. Blatt. 1994. Peptides derived from the auxin binding protein elevate Ca^{2+} and pH in stomatal guard cells of *Vicia faba*: a confocal fluorescence ratio imaging study. *Symp. Soc. Exp. Biol.* 48:215–228.

Frohnmeyer, H., A. Grabov, and M.R. Blatt. 1998. A role for the vacuole in auxin-mediated control of cytosolic pH by *Vicia* mesophyll and guard cells. *Plant J.* 13:109–116.

Gibbon, B.C., and D.L. Kropf. 1991. pH gradients and cell polarity in *Pelvetia* embryos. *Protoplasma.* 163:43–50.

Gibbon, B.C., and D.L. Kropf. 1994. Cytosolic pH gradients associated with tip growth. *Science*. 263:1419–1421.

Gluck, S., C. Cannon, and Q. Al-Awqati. 1982. Exocytosis regulates urinary acidification in turtle bladder by rapid insertion of H^+ pumps into the luminal membrane. *Proc. Natl. Acad. Sci. USA*. 79:4327–4331.

Grandin, N., and M. Charbonneau. 1991. Intracellular free calcium oscillates during cell division of *Xenopus* embryos. *J. Cell Biol.* 112:711–718.

Gray, P., and S.K. Scott. 1990. Chemical oscillations and instabilities: Non-linear chemical kinetics. Clarendon Press, Oxford, UK. 453 pp.

Guern, J., H. Felle, Y. Mathieu, and A. Kurkdjian. 1991. Regulation of intracellular pH in plant cells. *Int. Rev. Cytol.* 127:111–173.

Harold, F.M., and J.H. Caldwell. 1990. Tips and currents: electrobiology of apical growth. *In* Tip Growth in Plant and Fungal Cells. I.B. Heath, editor. Academic Press, San Diego, CA. 59–90.

Hepler, P.K., and B. Gunning. 1998. Confocal fluorescence microscopy of plant cells. *Protoplasma.* 201:121–157.

Herrmann, A., and H.H. Felle. 1995. Tip growth in root hair cells of *Sinapsis alba* L.: significance of internal and external Ca^{2+} and pH. *New Phytol.* 129: 523–533.

Holdaway-Clarke, T., J.A. Feijó, G.R. Hackett, J.G. Kunkel, and P.K. Hepler. 1997. Pollen tube growth and the intracellular cytosolic calcium gradient oscillate in phase while extracellular calcium influx is delayed. *Plant Cell.* 9:1999–2010.

Jaffe, L.F. 1977. Electrophoresis along cell membranes. *Nature*. 265:600–602.

Jiang, C.-J., A.G. Weeds, S. Khan, and P.J. Hussey. 1997. F-actin and G-actin binding are uncoupled by mutation of conserved tyrosine residues in maize actin depolymerization (*Zea* ADF). *Proc. Natl. Acad. Sci. USA*. 94:9973–9978.

Jolicoeur, M., S. Germette, M. Gaudette, M. Perrier, and G. Bécard. 1998. Intracellular pH in arbuscular mycorrhizal fungi. *Plant Physiol.* 116:1279–1288.

Kasner, S.E., and M.B. Ganz. 1992. Regulation of intracellular potassium in mesangial cells: a fluorescence analysis using the dye, PBFI. *Am. J. Physiol*. 262:F462–F467.

Kim, S.R., Y. Kim, and G. An. 1993. Molecular cloning and characterization of anther-preferential cDNA encoding a putative actin-depolymerization factor. *Plant Mol. Biol.* 21:39–45.

Kinoshita, T., M. Nishimura, and K.-I. Shimazaki. 1995. Cytosolic concentration of Ca^{2+} regulates the plasma membrane H^+-ATPase in guard cells of fava bean. *Plant Cell*. 7:1333–1342.

Kochian, L.V., J.E. Shaff, W.M. Küthreiber, L.F. Jaffe, and W.J. Lucas. 1992. Use of an extracellular, ion-selective, vibrating microelectrode system for the quantification of K^+, H^+ and Ca^{2+} fluxes in maize roots and maize suspension cells. *Planta*. 188:601–610.

Kost, B., P. Spielhofer, and N.-H. Chua. 1998. A GFP-mouse talin fusion protein labels plant actin filaments in vivo and visualizes the actin cytoskeleton in growing pollen tubes. *Plant J.* 16:393–401.

Kropf, D.L., C.A. Henry, and B.C. Gibbon. 1995. Measurement and manipulation of cytosolic pH in polarizing zygotes. *Eur. J. Cell Biol.* 68:297–305.

Kühtreiber, W.M., and L.F. Jaffe. 1990. Detection of extracellular calcium gradients with a calcium-specific vibrating electrode. *J. Cell Biol.* 110:1565–1573.

Lino, B., V.M. Baizabal-Aguirre, and L.E.G. de la Vara. 1998. The plasma membrane H^+-ATPase from beet root is inhibited by a calcium-dependent phosphorylation. *Planta.* 204:352–359.

Lopez, I., R.G. Anthony, S.K. Maciver, C.J. Jiang, S. Khan, A.G. Weeds, and P.J. Hussey. 1996. Pollen specific expression of maize genes encoding actin depolymerizing factor-like proteins. *Proc. Natl. Acad. Sci. USA*. 93:7415–7420.

Malhó, R., N.D. Read, A.J. Trewavas, and M.S. Pais. 1994. Role of cytosolic free calcium in the reorientation of pollen tube growth. *Plant J.* 5:331–341.

Malhó, R., N.D. Read, M.S. Pais, and A.J. Trewavas. 1995. Calcium channel activity during pollen tube growth and reorientation. *Plant Cell.* 7:1173–1184.

Malhó, R., and A.J. Trewavas. 1996. Localized apical increases of cytosolic free calcium control pollen tube orientation. *Plant Cell.* 8:1935–1949.

Messerli, M., and K.R. Robinson. 1997. Tip localized Ca^{2+} pulses are coincident with peak pulsatile growth rates in pollen tubes of *Lilium longiflorum*. *J. Cell. Sci.* 110:1269–1278.

Messerli, M., and K.R. Robinson. 1998. Cytoplasmic acidification and current influx follow growth pulses of *Lilium longiflorum* pollen tubes. *Plant J.* 16: 87–91.

Miller, D.D., D.A. Callaham, D.J. Gross, and P.K. Hepler. 1992. Free Ca^{2+} gradient in growing pollen tubes of *Lilium*. *J. Cell Sci.* 101:7–12.

Miller, D.D., S.A. Lancelle, and P.K. Hepler. 1996. Actin microfilaments do not form a dense meshwork in *Lilium longiflorum* pollen tube tips. *Protoplasma.* 195:123–132.

Moon, A., and D.G. Dubin. 1995. The ADF/cofilin proteins: stimulus-responsive modulators of actin dynamics. *Molec. Biol. Cell.* 6:1423–1431.

Murray, J.D. 1993. Mathematical Biology. Springer-Verlag, Berlin, Germany. 767 pp.

Murray, J.W., B.T. Edmonds, G. Liu, and J. Condeelis. 1996. Bundling of actin filaments by elongation factor 1α inhibits polymerization at filament ends. *J. Cell Biol.* 135:1309–1321.

Nuccitelli, R. 1983. Transcellular ion currents: signals and effectors of cell po-

larity. *Mod. Cell Biol.* 2:451–481.
Obermeyer, G., M. Lützelschwab, H.G. Heumann, and M.H. Weisenseel. 1992. Immunolocalization of H^+-ATPases in the plasma membrane of pollen grains and pollen tubes of *Lilium longiflorum*. *Protoplasma*. 171:55–63.
Obermeyer, G., and M.H. Weisenseel. 1991. Calcium channel blockers and calmodulin antagonists affect the gradient of free calcium ions in lily pollen tubes. *Eur. J. Cell Biol.* 56:319–327.
Opas, M. 1997. Measurement of intracellular pH and pCa with a confocal microscope. *Trends Cell. Biol*. 7:75–80.
Parton, R.M., S. Fischer, R.M. Malhó, O. Papasouliotis, T.C. Jellito, T. Leonard, and N.C. Read. 1997. Pronounced cytoplasmic gradients are not required for tip growth in plant and fungal cells. *J. Cell Sci*. 110:1187–1198.
Pawley, J.B. 1995. Fundamental limits in confocal microscopy. *In* Handbook of Biological Confocal Microscopy. 2nd ed. J.B. Pawley, editor. Plenum Press, New York. 19–38.
Pierson, E.S., D.D. Miller, D.A. Callaham, A.M. Shipley, B.A. Rivers, M. Cresti, and P.K. Hepler. 1994. Pollen tube growth is coupled to the extracellular calcium ion flux and the intracellular calcium gradient: effect of BAPTA-type buffers and hypertonic media. *Plant Cell.* 6:1815–1828.
Pierson, E.S., D.D. Miller, D.A. Callaham, J. van Aken, G. Hackett, and P.K. Hepler. 1996. Tip-localized calcium entry fluctuates during pollen tube growth. *Dev. Biol.* 174:160–173.
Poenie, M. 1990. Alteration of intracellular Fura-2 fluorescence by viscosity: a simple correction. *Cell Calcium*. 11:85–91.
Rathore, K.S., R.J. Cork, and K.R. Robinson. 1991. A cytoplasmic gradient of Ca^{2+} is correlated with the growth of lily pollen tubes. *Dev. Biol.* 148:612–619.
Ravesloot, J.H. 1998. Strategies for studying intracellular pH regulation. *In* Signal Transduction-Single Cell Techniques. B. van Duijn and A. Wiltink, editors. Springer-Verlag, Berlin, Germany. 468 pp.
Robson, G.D., E. Prebble, A. Rickers, S. Hosking, D.W. Denning, A.P.J. Trinci, and W. Robertson. 1996. Polarized growth of fungal hyphae is defined by an alkaline pH gradient. *Fungal Genet. Biol.* 20:289–298.
Smith, F.A., and R.J. Reid. 1991. Biophysical and biochemical regulation of cytoplasmic pH in *Chara corallina* during acid load. *J. Exp. Bot*. 42:173–182.
Smith, P.J.S., R.H. Sanger, and L.F. Jaffe. 1994. The vibrating Ca^{2+}electrode: a new technique for detecting plasma membrane regions of Ca^{2+} influx and efflux. *Methods Cell Biol*. 40:115–134.
Stern, M.D. 1992. Buffering of calcium in the vicinity of a channel pore. *Cell Calcium.* 13:183–192.
Suprenant, K.A. 1991. Unidirectional microtubule assembly in cell-free extracts of *Spisula solidissima* oocytes is regulated by subtle changes in pH. *Cell Motil. Cytoskel.* 19:207–220.
Sze, H. 1985. H^+-Translocating ATPases: advances using membrane vesicles. *Annu. Rev. Plant Physiol*. 36:175–208.
Turian, G. 1981. Decreasing pH-gradient toward the apex of germinating pollen tubes. *Bot. Helv*. 91:161–167.
Turing, A. 1952. The chemical basis of morphogenesis. *Philo. Trans. Roy. Soc. Lond. Ser.* B237:5–72.
Weisenseel, M.H., and L.F. Jaffe. 1976. The major growth current through the lily pollen tube enters as K^+ and leaves as H^+. *Planta.* 133:1–7.
Yang, X.-C., and F. Sachs. 1989. Block of stretch-activated ion channels in *Xenopus* oocytes by gadolinium and calcium ions. *Science*. 243:1068–1071.
Yonezawa, N., E. Nishida, and H. Sakai. 1985. pH control of actin polymerization by cofilin. *J. Biol. Chem.* 260:14410–14412.